Transaction of the Korean Nuclear Society Spring Meeting
Jeju, Korea, May 17-19, 2017

Fabrication of Neutron Absorber Containing Ceramic Composite Pellets by using Microwave Sintering

Qusai Mistarihi[1], Wooseong Park[2], Kyungseok Nam[2], Mohd-Syukri Yahya[1], Yonghee Kim[1], and Ho Jin Ryu[1]*
[1]*Korea Advanced Institute of Science and Technology, Nuclear & Quantum Engineering Dept. 291 Daehakro, Yuseong, 34141, Republic of Korea*
Kyunghee university, Nuclear Engineering Department, Kyungheedae-ro, Dongdaemun-gu, Seoul, 02447, Republic of Korea
[*]*Corresponding author: hojinryu@kaist.ac.kr*

1. Introduction

To improve the reactor performance through longer fuel cycle lengths and higher burnup, an excess amount of reactivity needs to be added to compensate for fuel depletion, fission product poisons build-up, and the loss of reactivity due to the changes in fuel temperature [1]. This amount of excess of reactivity needs to be controlled in order to prevent supercriticality. The main control mechanisms for Light Water Reactors (LWRs) are control rods, chemical shim in the form of boric acid dissolved in the coolant, and Burnable Absorbers (BAs) [2]. Using control rods to compensate for this excess of reactivity produces non-uniform power distribution [3] and the excess of reactivity cannot be indefinitely compensated for by the use of chemical shim; because the concentration of boric acid in the nuclear reactor is limited as beyond a certain concentration, the thermal expansion of the water reduces the quantity of Boron in the core and result in a positive moderator temperature reactivity coefficient (MTC) [4]. One way to compensate for this excess of reactivity is the use of BA.

The main requirements for BA materials are: (1) a high neutron absorption cross section; (2) a burnout rate matching fuel depletion, and (3) the absence of strongly neutron-absorbing radioisotopes [5]. BAs can be classified into two categories; boron containing materials and rare earth oxides. Due to He gas emission, high sintering temperature, and the relatively low neutron absorption cross section, boron-containing materials are usually applied as a coating on fuel pellets as used in Integral Fuel Burnable Absorber (IFBA) [6] or in separate fuel pellets like Wet Annular Burnable Absorber (WABA) [7]. Rare earth oxides have a high neutron absorption cross section and relatively lower sintering temperature and therefore can be mixed with uranium oxide fuel [8]. Urania-Gadolinia mixed oxide fuel is widely used as BA; because it offers decreased water displacement and reduced handling and personnel exposure [9]. A more effective reactivity control can be achieved by lumping Gd_2O_3 into UO_2 to achieve a higher self-shielding of the BA. Having a higher self-shielding of the BA will reduce the effective absorption cross section of the BA to minimize the reactivity mismatch at the beginning of life cycle and increase it as the fuel depletes in order to maintain the reactivity as high as possible at the end of the life cycle [10]. Fleming et al. calculated the self-shielding factor for spherical, cylindrical and slab geometry neutron absorber by solving the neutron transport equation for mono-energetic isotropic neutron flux and found that the spherical BA has a higher self-shielding than the cylinder than the slab due to its higher surface area and therefore a better reactivity control [11]. Yahya et al. [12] found that a lumped Gd_2O_3 in the center of the fuel rod had a better neutronic performance than the conventional urania-gadollinia fuel.

There are two fabrication methods for urania- gadolinia mixed oxide fuel; dry mechanical milling and co-precipitation. The dry mechanical milling is mostly employed due to its simplicity. In the dry mechanical milling, UO_2 and Gd_2O_3 powder are firstly mixed in 1:1 ratio using shaker mixer and after that, the mix is added to the bulk UO_2 and homogenized. Then, the homogenized mixture is pressed to 50 % theoretical density and finally sintered at 1650^{o}C for 3 h in H_2 atmosphere using the conventional sintering method [4]. Lower sintering temperature and shorter sintering time can be achieved using non-conventional sintering methods like MW and Spark Plasma Sintering (SPS) [13-14].

The objective of this study is to investigate the fabricability of ceramic pellets containing lumped Gd_2O_3 sphere, rod, mini-pellet using Microwave (MW) sintering for the application of new BA design. Fig. 1 shows a schematic diagram for proposed designs. Firstly, the sinterability of Yttrium stabilized ZrO_2 (YSZ) and Gd_2O_3 by MW was investigated. Secondly, we investigated the effect of Gd_2O_3 doping with 8YSZ on Gd_2O_3 densification by MW, stabilization of Gd_2O_3 cubic structure, and on the thermal conductivity of Gd_2O_3. Finally, we investigated the fabricability of ceramic pellets containing lumped Gd_2O_3 rod, mini-pellet, and sphere using YSZ as a surrogate for UO_2.

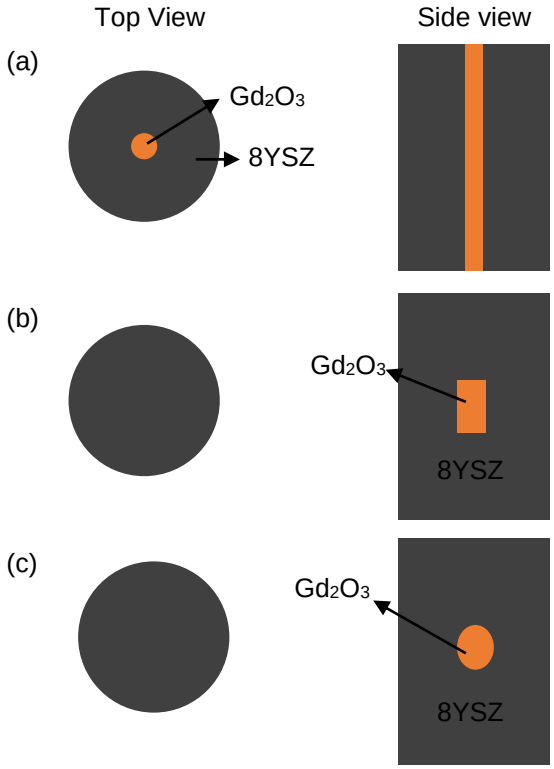

Fig. 1. Schematic diagram for ceramic fuel pellet containing (a) Gd_2O_3 rod, (b) mini-pellet, and (c) sphere.

2. Experimental procedures:

2.1 Starting materials

ZrO_2- 8 mol. % Y_2O_3 (8YSZ) (Sigma Aldrich, 99.9 %, ~ 700 nm), Gd_2O_3 (Alpha Aesar, 99.9 %, < 10 µm), Alginic acid sodium salt (Sigma Aldrich) with 15-25 cP viscosity for 1 wt.% in H_2O, $CaCl_2$ solution (Sigma Aldrich, 1 M) were used as starting materials.

2.2 Gd_2O_3-x wt. % 8YSZ composites

In order to investigate the sinterability of Gd_2O_3 and 8YSZ using MW sintering, 8YSZ and Gd_2O_3 powder were uni-axially pressed under a pressure of 33.5 MPa followed by Cold isostatic pressing under a pressure of 400 MPa, and finally sintered in air using MW sintering at 1400-1600°C for 20 min.

Pure Gd_2O_3 and Gd_2O_3 doped with 2, 5, 10, and 20 wt. % of 8YSZ composites were fabricated to investigate the effect of 8YSZ doping on the crystal structure of Gd_2O_3, its densification by MW, and its thermal conductivity. The required amounts of Gd_2O_3 and 8YSZ were mixed suing 3D mixer in 70 ml of ethanol for 3 h using 2 mm ZrO_2 balls and a ball to powder ratio of 1:10 at a mixing speed of 40 rpm. The mixture was dried at 120°C for 12 h and used to fabricate Gd_2O_3-x wt.% YSZ composites by uni-axially pressing under a pressure of 55.5 MPa, and then Cold isostatically pressing under a pressure of 400 MPa, and MW sintering of the green pellets at 1500°C for 20 min in an air atmosphere.

The microstructure of the sintered composites was characterized using Scanning Electron Microscopy (SEM) and Energy-dispersive X-ray analysis (EDAX). The crystal structure was analyzed using X-ray Diffractometry (XRD) and the densification was measured using Archimedes principle. The thermal conductivity of the sintered composites at different temperature was calculated from the experimentally measured density, heat capacity, and thermal diffusivity. The thermal diffusivity was measured using the laser flash method (LFA 457, NETZSCH) and the heat capacity was measured using scanning calorimetry (DSC 404 C, NETZSCH). The density of the sintered samples at different temperatures was calculated from the thermal expansion coefficients and the measured density at room temperature.

2.3 Fabrication of oxide pellets containing Gd_2O_3 rod and mini-pellet

An annular steel mold with an inner hole diameter of 2 mm and an outer cavity diameter of 10 mm was manufactured in order to fabricate the ceramic pellets.

For Gd_2O_3 rod containing oxide pellets, 8YSZ powder was poured into the annular mold and uni-axially pressed under a pressure of 59 MPa. Then, Gd_2O_3 powder was poured in the center hole of the YSZ annular pellet and pressed under the same pressure using a steel rod.

For Gd_2O_3 mini-pellet containing oxide pellets, 1/3 of the total amount of 8YSZ powder was firstly poured in the annular mold and uni-axially pressed under a pressure of 59 MPa followed by pouring Gd_2O_3 powder in the center hole of the YSZ annular pellet and pressing under the same pressure using a steel rod. Then, the other 2/3 of the total amount of 8YSZ powder were poured in the annular mold and ui-axially pressed under a pressure of 57 MPa.

The uni-axially pressed pellet was cold isostatically pressed at 400 MPa for 5 min. to fabricate green pellets. The green pellets were sintered using MW sintering at 1500°C for 20 minutes. The microstructure of the sintered pellets was characterized using SEM and EDAX.

2.4 Fabrication of oxide pellets containing Gd_2O_3 sphere

Firstly, Gd_2O_3 spheres were fabricated using the drip casting method by dripping Gd_2O_3-based sodium alginate slurry into $CaCl_2$ solution. The slurry was prepared by adding 25-75 wt. % of Gd_2O_3 powder to water under continuous mixing and then adding 3-5 wt.% of sodium alginate and continue mixing until all sodium alginate was dissolved. The prepared slurry was dripped from different heights into the $CaCl_2$ solution using a syringe with 1 and 2 mm tip size. Then, the synthesized Gd_2O_3 spheres were washed with water for 30 min to remove extra Ca and dried after washing at a temperature of 120°C for 12 h to remove the remaining water. The effect of Gd_2O_3 content, sodium alginate content, dripping height, and the tip size of the syringe on the sphericity and size of Gd_2O_3 spheres were investigated in order to find the optimum parameters

for the fabrication of Gd_2O_3 spheres. After that, the fabricated spheres were sintered using a box furnace at 1500-1600ºC for 2 h in air with a heating rate of 5ºC/min up 1000ºC and 10ºC/min from 1000ºC to the sintering temperature. SEM and EDAX analyzed the microstructure of the sintered and dried spheres. The sphericity was calculated from the ratio of the short diameter and the long diameter of the spheres and the size was calculated from the average value of them. The diameter of the sphere was measured using a caliper. At least five measurements were performed.

secondly, the oxide fuel pellets containing sintered and dried Gd_2O_3 spheres were fabricated by firstly pouring half of the total amount of 8YSZ inside a steel mold of 10 mm diameter. Then punching the pellet with a 2 mm steel rod and inserting the Gd_2O_3 sphere. Finally, pouring the other half in the steel mold and uni-axially pressing under a pressure of 57 MPa to prepare the green pellets. Then the green pellets were cold-isostatically pressed and MW sintered using the same conditions for the oxide pellets containing Gd_2O_3 mini-pellet and rod.

3. Results and discussion

Figure 2 and Figure 3 show the effect of the sintering temperature on the densification of Gd_2O_3 and 8YSZ. MW sintering was more effective in sintering 8YSZ than Gd_2O_3 with a relative density at 1600ºC of 98.4 % and 94.6 % for 8YSZ and Gd_2O_3 respectively. This is due to the higher dielectric constant for MW [15-16] and the smaller particle size of YSZ than that of Gd_2O_3.

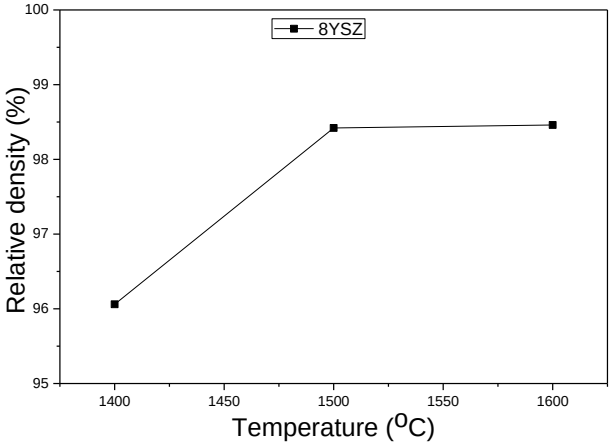

Fig. 2. The effect of sintering temperature on the densification of 8YSZ by MW

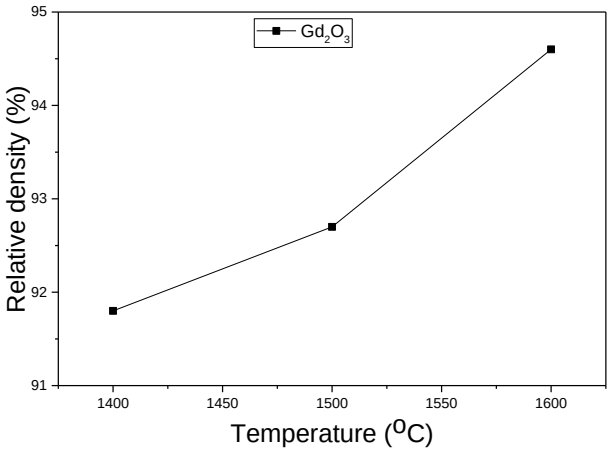

Fig. 3. The effect of sintering temperature on the densification of Gd_2O_3 by MW.

The density of 8YSZ increased with increasing the sintering temperature from 1400 to 1500ºC and then remained almost constant after increasing the sintering temperature to 1600ºC. On the other hand, the density of Gd_2O_3 increased gradually with increasing the sintering temperature. Upadhyaya et al. [17] and Mazaheri et al. [18] sintered 8YSZ using MW sintering and found that a densification of 97 % for powder sintered at 1540ºC for 35 minutes with an average particle size of 0.69 µm [16] and 97.5 % for powder sintered at 1500ºC with an average particle size of 33 nm was achieved [18] which is comparable to our study where a 98.4 % densification was achieved for 8YSZ powder with 700 nm average particle size when sintered at 1500ºC for 20 min. There is no study about the sinter-ability of Gd_2O_3 by MW sintering and the studies about the sintering of bulk Gd_2O_3 are scarce. Only one study was recently published about the sinterability of Gd_2O_3 using SPS [19]. In this study, Gd_2O_3 was about 92.5% densified when the sintering temperature was 1500ºC. The neutronic performance analysis of Gd_2O_3-cored fuel with 80 % densified Gd_2O_3 showed a better reactivity control than the conventional urania-gadolinia fuel [12]. The partially densified Gd_2O_3 can also accommodate the nuclear fission products.

X-ray diffraction patterns for Gd_2O_3 and 8YSZ powders and pellets sintered at different sintering temperature are shown in Figure 4 and 5.

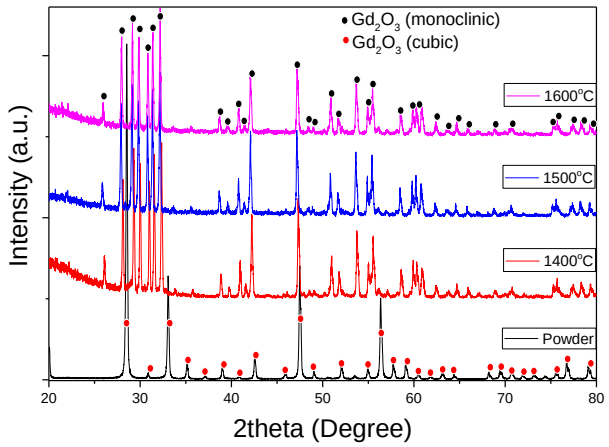

Fig. 4. X-Ray diffraction patterns for Gd_2O_3 powders and sintered Gd_2O_3 pellets.

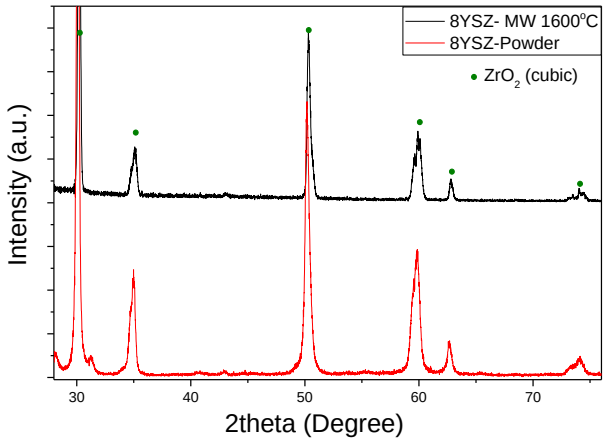

Fig. 5. X-Ray diffraction patterns for Powders and sintered 8YSZ pellets

Gd_2O_3 exists in three different crystal structures; cubic, monoclinic, and hexagonal. At room temperature, Gd_2O_3 has the cubic structure and at about 1250°C it transforms into monoclinic structure [20]. It was experimentally found that the cubic to monoclinic phase transformation was irreversible even with a slow cooling rate of 2°C/min [21]. The crystal structure of 8YSZ remained cubic after sintering at a temperature up to 1600°C indicating the stability of the cubic structure of 8YSZ at high temperature.

Figure 6 and 7 show the microstructure and the XRD diffraction pattern of 8YSZ doped Gd_2O_3 composites. The microstructure of 8YSZ doped Gd_2O_3 composites was composed of two phases (Fig. 6). The EDs mapping of the second phase showed that it was mainly composed of Gd, O and Zr. As can be seen from Figure 7, both of the monoclinic and cubic phase of Gd_2O_3 were observed for Gd_2O_3- 2 wt.% 8YSZ composites and no diffraction peaks for monoclinic Gd_2O_3 were observed when the wt.% of 8YSZ was 5 or above. At 10 wt.% or above of 8YSZ, the cubic like Gd_2ZrO_5 oxide solid solution was observed.

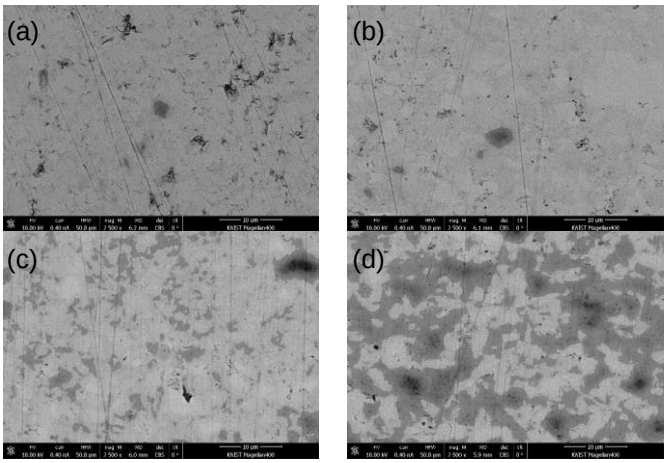

Fig. 6. SEM microstructure of Gd_2O_3 doped with (a) 2, (b) 5, (c) 10, and (d) 20 wt.% of 8YSZ

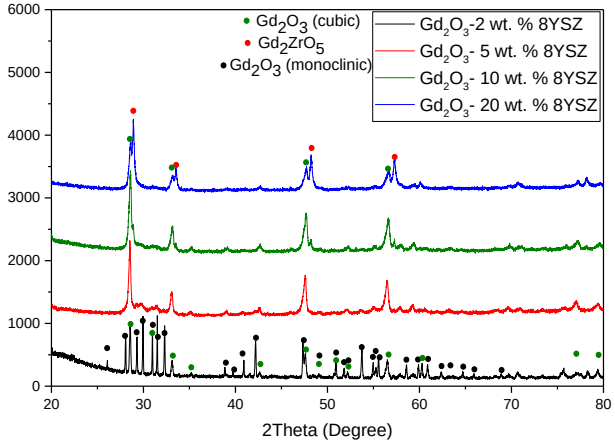

Fig. 7. XRD diffraction pattern of 8YSZ doped Gd_2O_3 composites.

Figure 8 and 9 show the relative density at room temperature and thermal conductivity of 8YSZ-doped Gd_2O_3 as a function of 8YSZ wt.% at different tempreatures.

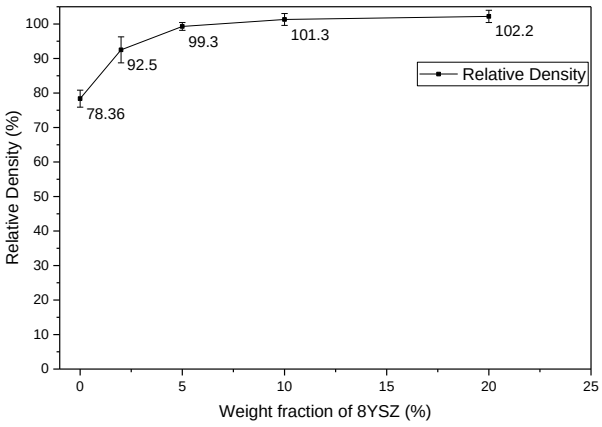

Fig. 8. Density of 8YSZ doped Gd_2O_3 composites

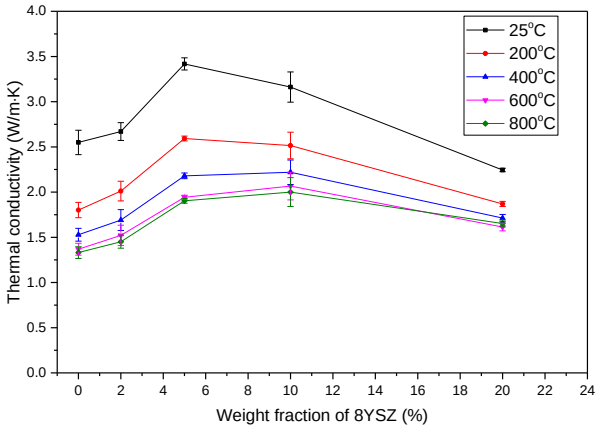

Fig. 9. Thermal conductivity of 8YSZ doped Gd_2O_3 composites as a function of 8YSZ wt.% at different temperatures.

The relative density of 8YSZ doped Gd_2O_3 composites increased with increasing the doping amount of 8YSZ and a densification of 99.3±1.1 was achieved for Gd_2O_3 composites doped with 5 wt. % of 8YSZ (Figure 8). Above 5 wt. % of 8YSZ, the relative density of the 8YSZ doped Gd_2O_3 composites remained almost constant. The increased densification of the 8YSZ doped Gd_2O_3 composites could be attributed to the better MW sinterability of 8YSZ due to its higher dielectric constant and smaller particle size [15-16]. As can be seen from Figure 9, The thermal conductivity of the 8YSZ doped Gd_2O_3 composites increased almost linearly with the wt.% of 8YSZ up to 5 wt. % and this could be due to the enhanced densification of the doped composites. However, when wt.% of 8YSZ increased above 10 %, the thermal conductivity decreased even though the full densification was achieved and this is due to the formation of low thermal conductivity Gd_2ZrO_7 oxide solid solutions. The thermal conductivity of rare earth zirconates was reported to be ~ 30 % lower than the thermal conductivity of 7YSZ with a thermal conductivity of 2 W/m·K or less [22].

The microstructure of 8YSZ oxide pellets containing Gd_2O_3 rod and Gd_2O_3 mini-pellet is shown in Figure 10. An interfacial gap and an oxide solid solution composed of Gd, Zr and O were observed at the interface between Gd_2O_3 rod and 8YSZ annular pellet (Figure 10a, c). For 8YSZ pellet containing Gd_2O_3 mini-pellet, Gd_2ZrO_5 phase with no interfacial gap was observed at the interface between the Gd_2O_3 mini-pellet and 8YSZ annular pellet. The formation of an interfacial gap in the 8YSZ pellet containing Gd_2O_3 rod could be attributed to the internal stress developed while inserting the Gd_2O_3 in the inner core of the annular 8YSZ pellet.

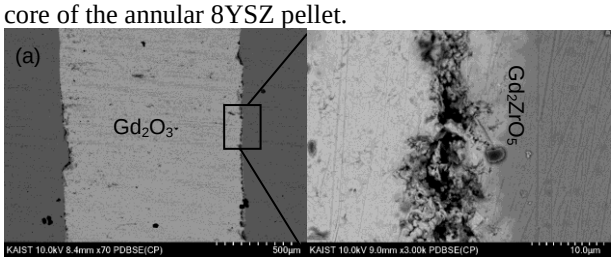

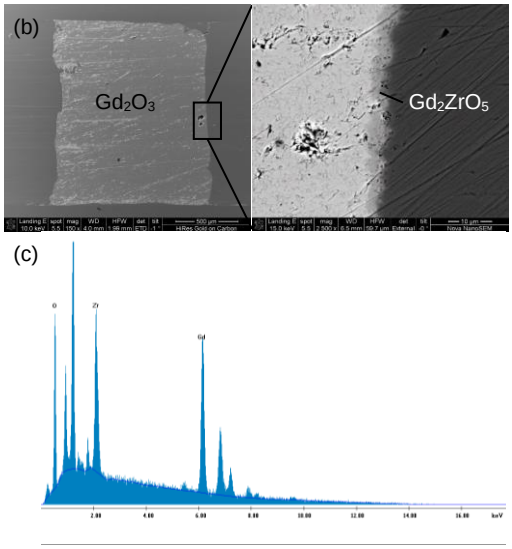

Fig. 10. SEM Microstructure of 8YSZ pellets containing (a) Gd_2O_3 rod and (b) Gd_2O_3 mini-pellet (c) EDS mapping of the oxide solid solution phase.

The formation process of beads is affected by several factors related to the alginate solution (surface, density, viscosity, sodium alginate concentration), gelling solution (surface tension, viscosity, concentration of Ca^{+2}), and mechanical parameters (tip size, dripping distance, collection distance) [23]. As the alginate solution is flowing from the nozzle, the droplet grows in size and once the gravitational force measured by the mass of the droplet is no longer balanced by the surface tension of the droplet, it falls down under the effect of gravitational force. During falling the shape of the droplet transform from tear shape, egg shape, and spherical shape regardless of the physical properties of the alginate solution. When the droplet reaches to the surface of the gelling solution, it will experience deformation that is controlled by the viscosity of the alginate solution droplet and the surface tension of the gelling solution. After the detachment from the surface of the gelling solution, the droplet will regain its spherical shape but its ability to regain its shape depends on its properties such as the viscosity and surface tension [23]. In this study the effect of sodium alginate concentration, Gd_2O_3 concentration, tip size, and dripping distance on the sphericity and size of Gd_2O_3 spheres were investigated and the results are shown in Table 1.

Table 1: Physical properties of dried Gd_2O_3 spheres

Sodium alginate content (wt.%)	Gd_2O_3 content (wt.%)	Tip size (mm)	Dripping distance (cm)	Sphericity (%)	Size (mm)
3	75	2	8	0.74±0.03	2.58±0.05
4	75	2	8	0.77±0.02	2.33±0.01
4	25	2	8	0.77±0.04	2.07±0.04
4	50	2	8	0.76±0.03	2.26±0.04
4	75	2	8	0.76±0.02	2.33±0.01
4	75	1	8	0.82±0.03	1.78±0.04
4	75	2	8	0.76±0.02	2.33±0.01
4	75	2	3	0.90±0.01	2.29±0.01

As can be seen from Table 1, the sphericity was found to be independent of the Gd_2O_3 concentration and dependent on the sodium alginate concentration, tip size, and dripping distance. The sphericity increased with increasing the sodium alginate concentration from 3 to 4 wt. %. Concentrations higher than 4 wt.% or less than 3 wt.% produced spheres with a tear shape. With the increase of the tip size from 1 to 2 mm, the sphericity decreased. The maximum sphericity of 90 % was achieved when the dripping distance was 3 mm. The size of the Gd_2O_3 was significantly affected by the size of the tip and sodium alginate concentration. The size of Gd_2O_3 spheres increased with increasing the tip size and decreasing the sodium alginate concentration. The optimum conditions for the fabrication of Gd_2O_3 spheres with highest sphericity, highest Gd_2O_3 content, and optimum size were 4 wt. % sodium alginate, 75 wt. % $Gd2O_3$, 3 cm dripping distance, and 2 mm tip size.

Figure 11 shows the microstructure of Gd_2O_3 spheres with the optimum fabrication conditions after drying and sintering. A porous microstructure was observed after drying and the porosity was decreased with sintering. However, after sintering a second phase composed mainly of Ca and Gd was observed in the microstructure of the sintered spheres at 1600ºC. This might be due to the short washing time of Gd_2O_3 spheres after gelation.

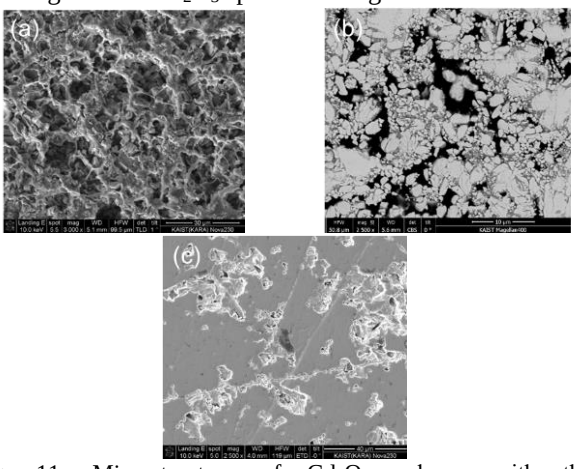

Fig. 11. Microstructure of Gd_2O_3 spheres with the optimum fabrication conditions after (a) drying and sintering at (b) 1500ºC and (c)1600ºC.

The microstructure of 8YSZ pellets containing dried and sintered Gd_2O_3 spheres is shown in Figure 12 and 13. An interfacial gap was observed in the 8YSZ pellets containing dried Gd_2O_3 spheres due to the shrinkage of the Gd_2O_3 sphere during sintering (Figure 12). On the other hand, a perfect interface without an interfacial gap was observed for 8YSZ pellets containing sintered Gd_2O_3 spheres (Figure 13). A Ca alginate rich phase was observed in the microstructure of the sintered Gd_2O_3 sphere (Figure 13b, c) indicating the short washing time for the Gd_2O_3 spheres

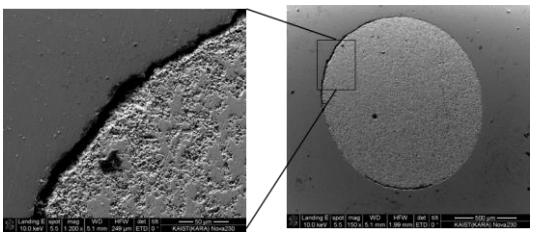

Fig. 12. Microstructure of 8YSZ pellets containing dried Gd_2O_3 spheres

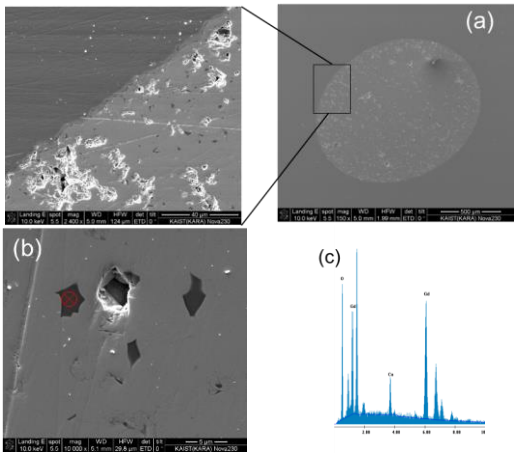

Fig. 13. Microstructure of 8YSZ pellets containing sintered Gd_2O_3 spheres showing (a) the interface between Gd_2O_3 sphere and 8YSZ pellets, (b) the high magnification microstructure and, (c) the EDS mapping for the second phase.

4. Conclusions

MW sintering of Gd_2O_3 and 8YSZ composites was investigated. The results showed that the 8YSZ had a better sinterability and no phase transformation after MW sintering at temperatures up to 1600ºC due to its higher dielectric constant and smaller particle size. On the hand, Gd_2O_3 showed a lower densification and an irreversible phase transformation from the cubic to the monoclinic phase.

Doping Gd_2O_3 with 8YSZ had a significant impact on its properties. The densification of Gd_2O_3 was improved with increasing the wt.% of 8YSZ and a full densification was observed at 5 wt.% or above. The cubic phase of Gd_2O_3 was found to be stabilized with the doping of 8YSZ. However, the cubic phase like Gd_2ZrO_5 oxide solid solution was started to appear at wt. % of 10 or above. The thermal conductivity of the doped composites was found to be increased with the increase of doping amount of 8YSZ up to 5 wt.% due to the improved densification. After that, the thermal conductivity decreased with the increase of the doping amount above 10 wt.% due to the formation of a low thermal conductivity Gd_2ZrO_5 oxide solid solution.

Gd_2O_3 spheres were fabricated by the drip casting method of Gd_2O_3 based sodium alginate slurry into $CaCl_2$ solution. The optimum conditions for the fabrication of Gd_2O_3 spheres were found to be 3 cm dripping distance, 2 mm tip size and 4 wt.% of sodium alginate. The size and sphericity of the dried Gd_2O_3 spheres fabricated with optimum conditions were about 2.3 mm and 90 % respectively. With increasing the sintering temperature of

Gd2O3 spheres from 1500 to 1600°C, the densification was increased. However, A Ca-rich phase was observed in the microstructure of the 1600°C sintered spheres due to the short washing time. In order to remove the Ca alginate, a longer washing time will be performed.

The fabrication of ceramic fuel pellets containing Gd_2O_3 rod, mini-pellet, and sphere using microwave sintering was investigated. An interfacial gap due to the internal stress developed during pressing Gd_2O_3 rod and Gd_2ZrO_5 phase were observed in the microstructure of 8YSZ pellet containing Gd_2O_3 rod. Gd_2ZrO_5 phase was observed in the microstructure of 8YSZ pellet containing Gd_2O_3 mini-pellets. No interfacial gap was observed in 8YSZ pellets containing sintered Gd_2O_3 spheres.

Acknowledgments

This study was supported by KUSTAR-KAIST institute of KAIST

REFERENCES

[1]Nicholas Tsoulfandidis. The nuclear fuel cycle. American nuclear society, La Grange Park (2013) 93-95.

[2]M. Ma. Benjamin. Nuclear reactor materials and applications. Iowa State University (1983) 377.

[3] V. S.Volkov, A. S. Luk'yanov, V. V. Chapkunov, V. P. Shevyakov, and V. S. Yamnikov, Use of burnable poisons in nuclear reactors, The Soviet Journal of Atomic Energy,Vol. 11-2, PP. 745-757, 1962.

[4]IAEA, Characteristics and use of urania-gadolinia fuels, TECDOC-844,1995.

[5] R. Manzel and W. Dorr, Manufacturing and Irradiation experience with UO2/Gd2O3 fuel, Journal of the American Ceramic Society, Vol. 59-6, P.601, 1980.

[6]K. Radford, B Argail, H. Keller, and R. Goodspeed, Fabrication development and application of an annular Al2O3-B4C burnable absorber, Nuclear Technology, Vol. 60, P. 344, 1983.

[7] R. Simmons, N. Jones, F. D. Popa, D. Mueller, and J Pritchett, Integral fuel burnable absorber with ZrB2 in pressurized water reactors, Nuclear Technology, Vol. 80, P. 343, 1988.

[8] M. Asou and J. Porta, Prospects for poisoning reactor cores of the future, Nuclear Engineering and Design, Vol. 168 P. 261, 1997.

[9]L. Goldstein, and Alfred A. Strasser, A comparison of gadolinia and boron for burnable poison applications in pressurized water reactors, Nuclear Technology, Vol. 60, PP. 352-36, 1983.

[10]James J Duderstadt, and Loius J. Hamilton. Nuclear reactor analysis. Vol. 84. New York: Wiley (1976) 553

[11] Ronlad F. Fleming, Neutron self-shielding for simple geometries, The International Journal of applied Radiation and Isotopes, Vol. 33-11, 1263-1268, 1982.

[12] M.Yahya, D.Hartanto, and Y. Kim, A neutronic study on annular fuel filled with burnable absorber, American nuclear society winter meeting, Nov.8-12, 2015, Washigton DC.

[13]Lihao Ge, Ghatu Subhash, Ronald H. Baney, and James S. Tulenko, Influence of processing parameters on thermal conductivity of uranium dioxide pellets prepared by spark plasma sintering, Journal of the European Ceramic Society, Vol.34-7, 1791-1801, 2014.

[14] Jae Ho Yang, Kun Woo Song, Yong Woo Lee, Jong Heon Kim, Ki Won Kang, Keon Sik Kim, and Youn Ho Jung, Microwave process for sintering of uranium dioxide, Journal of nuclear materials, Vol. 325- 2, 210-216, 2004.

[15] M. Lanagan, J. Bhalla, and S. Sankar, The dielectric properties of yttria stabilized zirconia, Materials Letters, Vol. 7, P. 12, 1989.

[16] G. Adachi, N. Imanaka, and Z. Kang, Binary Rare Earth Oxides, Kluwer Academic Publisher, New York, P. 117, 2004.

[17] D. Upadhyaya, A. Ghosh, K. Gurumurthy, and R. Prasad, Microwave sintering of cubic zirconia, Ceramic international, Vol. 27, P. 415, 2001.

[18] M. Mazaheri, A. Zahedi, and M. Hejazi, Processing of nanocrystalline 8 mol% yttria-stabilized zirconia by conventional, microwave-assisted and two step sintering, Materials Science Engineering A, Vol. 492, P. 261, 2008.

[19] E. Awin, S. Sridar, R.Shabadi, and R. Kumar, Structural, functional and mechanical properties of spark plasma sinterd gadolinia, Ceramic international, Vol. 42, P. 1384, 2016.

[20] W. Shafer and R. Roy, Rare earth polymorphism and phase equilibria in rare-earth oxide water system, Journal of the American Ceramic Society, Vol. 42, P. 563, 1959.

[21] R. Roth and S. Schneider, Phase equilibria in systems involving the rare-earth oxides. Part I. polymorphism of the oxides of the trivalent rare-earth ions, Journal of the Research of the national Bureau of standards-A Physics and Chemistry, Vol. 64, P. 309, 1960.

[22] J. Wu, Xuezheng Wei, Nitin P. Padture, Paul G. Klemens, Maurice Gell, Eugenio García, Pilar Miranzo, and Maria I. Osendi, Low-Thermal-Conductivity Rare-Earth Zirconates for Potential Thermal-Barrier-Coating Applications, Journal of the American Ceramic Society, Vol. 85-12, PP. 3031-3035, 2002.

[23] B-B. Lee, Pogaku Ravindra, and E-S. Chan, Size and shape of calcium alginate beads produced by extrusion dripping, Chemical Engineering & Technology, Vol. 36, PP. 1627-164, 2013.